Physica D 239 (2010) 766–775

Contents lists available at ScienceDirect

Physica D

journal homepage: www.elsevier.com/locate/physd

Anomalous dispersion in the Belousov–Zhabotinsky reaction: Experiments and modeling

Grigory Bordyugov [a,*], Nils Fischer [b,1], Harald Engel [b], Niklas Manz [c,2], Oliver Steinbock [c]

[a] Institut für Physik und Astronomie, Universität Potsdam, Karl-Liebknecht-Straße 24/25, 14476 Potsdam, Germany

[b] Institut für Theoretische Physik, Technische Universität Berlin, Hardenbergstraße 36, 10623 Berlin, Germany

[c] Florida State University, Department of Chemistry and Biochemistry, Tallahassee, FL 32306-4390, United States

ARTICLE INFO

Article history:
Available online 6 December 2009

Keywords:
Reaction–diffusion systems
Excitability
Orbit flip
Continuation methods

ABSTRACT

We report results on dispersion relations and instabilities of traveling waves in excitable systems. Experiments employ solutions of the 1,4-cyclohexanedione Belousov–Zhabotinsky reaction confined to thin capillary tubes which create a pseudo-one-dimensional system. Theoretical analyses focus on a three-variable reaction–diffusion model that is known to reproduce qualitatively many of the experimentally observed dynamics. Using continuation methods, we show that the transition from normal, monotonic to anomalous, single-overshoot dispersion curves is due to an orbit flip bifurcation of the solitary pulse homoclinics. In the case of "wave stacking", this anomaly induces attractive pulse interaction, slow solitary pulses, and faster wave trains. For "wave merging", wave trains break up in the wake of the slow solitary pulse due to an instability of wave trains at small wavelength. A third case, "wave tracking" is characterized by the non-existence of solitary waves but existence of periodic wave trains. The corresponding dispersion curve is a closed curve covering a finite band of wavelengths.

1. Introduction

Excitable reaction–diffusion systems show a remarkable wealth of spatio-temporal dynamics. Prominent examples include spirals, rotating scroll waves and turbulent states [1]. The primary building blocks of these structures are excitation pulses that, in the simplest case, have constant profiles and steady velocities. They exist in many experimental systems such as the CO oxidation on platinum surfaces, corrosion systems, the Belousov–Zhabotinsky (BZ) reaction, slime molds, neuronal and cardiac systems as well as mouse skin [2].

The latter systems have a stable steady state and undergo long excursions through phase space if triggered by a super-critical perturbation. Qualitatively this excitation cycle consists of an excited state followed by a slow recovery phase during which the excitation threshold is raised and the system is refractory. For traveling excitation pulses, this temporal behavior is unfolded in space. Consequently, the pulses have a trailing refractory zone in which the medium slowly recovers its excitability.

The specific features of this recovery process are a major factor in determining the velocity of infinite pulse trains. In many experimental systems, this velocity c increases monotonically with pulse spacing (or wavelength) L and saturates at a finite speed that equals the speed of a solitary pulse propagating into a fully recovered medium [3]. Moreover, there is a minimal pulse spacing below which no wave trains exist. This type of dependence is commonly referred to as "normal dispersion relation". Furthermore, it was shown that in certain cases the velocity varies as the hyperbolic tangent of the normalized period of the wave train [4].

Over two decades ago, numerical studies revealed the existence of anomalous dispersion relations which specifically involved a single overshoot or damped oscillations in $c(L)$ [5]. Both features can be understood qualitatively as consequences of non-monotonic recovery profiles [6,7]. Furthermore, Winfree showed that anomalous dispersion can allow spiral waves to rotate at more than one characteristic frequency [8]. In addition, more recent studies documented anomalies involving band-gaps and bistability [9]. Experimentally dispersion relations with a single overshoot were found in the catalytic reduction of NO with CO on platinum surfaces [10], a BZ-type reaction in which malonic acid is replaced by 1,4-cyclohexanedione (CHD) [11,12], and possibly the slime mold *Dictyostelium discoideum* [13]. We would also like to mention some recent publications on the attractive interaction between pulses [14] and on the interaction of pulses with pacemakers [15].

* Corresponding author. Tel.: +49 175 247 8282.
E-mail addresses: Grigory.Bordyugov@uni-potsdam.de (G. Bordyugov), steinbck@chem.fsu.edu (O. Steinbock).
[1] Present address: Max Planck Institute for Meteorology, Bundesstraße 53, 20146 Hamburg, Germany.
[2] Present address: Henri Begleiter Neurodynamics Laboratory, Department of Psychiatry and Behavioral Sciences, SUNY, Downstate Medical Center, 450 Clarkson Avenue, Brooklyn, NY 11203, United States.

0167-2789/$ – see front matter © 2009 Elsevier B.V. All rights reserved.
doi:10.1016/j.physd.2009.10.022

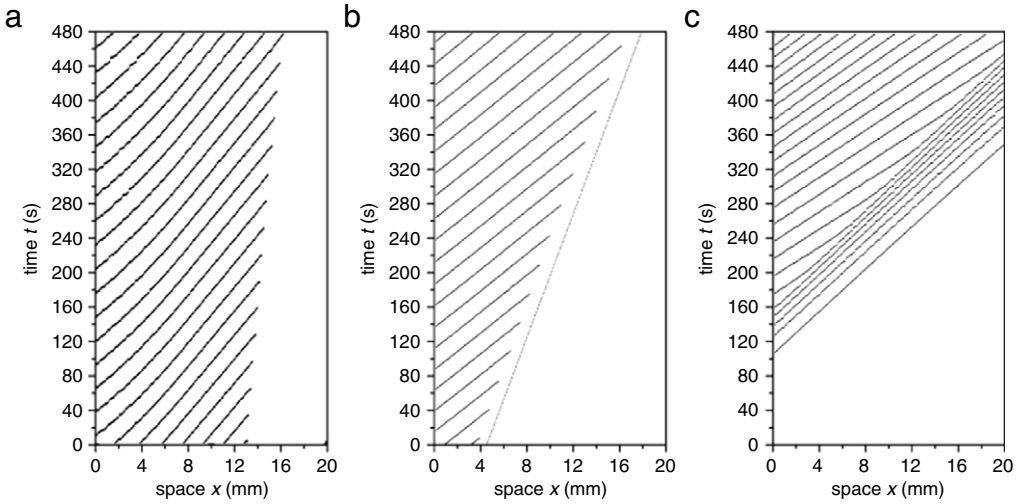

Fig. 1. Space–time front trajectories with tracking (a), merging (b), and stacking (c) dynamics. Initial concentrations: $[H_2SO_4] = 0.60$ M, $[CHD] = 0.20$ M, $[NaBrO_3] = 0.20$ M (a), 0.25 M (b), and 0.30 M (c), and $[Fe[batho(SO_3)_2]_3] = 0.50$ mM.

This Article discusses three distinct types of wave dynamics in the CHD-BZ reaction and analyzes a reaction–diffusion model that qualitatively reproduces these phenomena. Specifically, we address questions relating to pulse stability and involved bifurcations using numerical continuation techniques.

2. Experimental

The classic BZ reaction involves the oxidation of malonic acid by bromate in an acidic solution and is catalyzed by redox-couples such as Ce(III)/Ce(IV). Our experiments are carried out with a modified BZ system in which malonic acid is replaced by 1,4-cyclohexanedione [16]. We use either ferroin ($Fe(phen)_3$) or $Fe[batho(SO_3)_2]_3$ [17] as redox catalyst. Experiments are performed at (24 ± 1) °C.

All solutions are prepared in nanopure water (18 MΩcm) obtained from a Barnstead EASYpure UV unit. We use the following stock solutions: 25 mM ferroin (Fluka, puriss. p.a.), 2.0 M sodium bromate (Fluka), and 0.5 M 1,4-cyclohexanedione (Aldrich). The latter solution is filtered through a Whatman 0.2 μm NYL filter. Sulfuric acid (5.0 M, Riedel-de Haën) is purchased as a standardized solution and used without further purification. The complex $Fe[batho(SO_3)_2]_3$ is prepared in a 25 mM sulfuric acid solution by mixing a 3:1 molar ratio of 4,7-diphenyl-1,10-phenanthrolinedisulfonic acid disodium salt hydrate (Acros) with ferrous sulfate heptahydrate (Fluka) to yield a 25 mM catalyst solution.

Our experiments employ thin glass capillaries as reaction containers (Drummond 20 μL MICROCAPS). Their inner diameter and length are 0.63 mm and 64 mm, respectively. A monochrome charge-coupled-device camera (COHU 2122) is used to monitor changes in the absorption profiles along the capillary tubes. The video signal is digitized with a low-noise image-acquisition card (Data Translation DT3155) to yield individual video frames of 640×480 pixel at 8 bits per pixel. These image data are acquired every $(0.25 - 1.00)$ s using commercial software (HLImage++97). Further analysis uses in-house programs written in IDL (Interactive Data Language, Research System Inc., Version 5.2).

3. Experimental results

Fig. 1 shows space–time plots that illustrate three qualitatively different regimes of wave dynamics in pseudo-one-dimensional CHD-BZ systems. The three experiments differ in the employed concentration of sodium bromate which was increased from 0.20 M in Fig. 1(a) to 0.30 M in Fig. 1(c). The individual space–time plots are constructed by piling up sequences of spatially one-dimensional absorption profiles. In the resulting data, each oxidation pulse is represented by a continuous band of low absorption values. The actual front positions of the individual pulses are measured as the space–time coordinates that are associated with largest spatial gradients and temporally decreasing absorption. Consequently, we obtain a trajectory $x_n(t)$ for each pulse where the index n counts subsequent pulses in increasing fashion. These trajectories are plotted in Fig. 1. All pulses are initiated at spontaneous pacemakers located slightly below $x = 0$. In these examples, all waves travel from the left to the right.

The space–time plots in Fig. 1 illustrate tracking (a), merging (b), and stacking (c) behavior. In the case of wave tracking, all pulses emitted into the medium vanish. However, each pulse travels farther than its predecessor and, hence, a large wave train can form. The expansion of this wave train depends strongly on the period of wave initiation. Furthermore, other experiments show that the wave train collapses but re-grows if the pacemaker stops intermittently. The expansion of a wave pattern in the tracking regime clearly involves a traveling boundary. This leading edge in itself behaves like a propagating front and connects the homogeneous rest state (right side of Fig. 1(a)) to the periodic pulse train. It has a distinctive but small propagation velocity which is reciprocal to the slope of the border between the waves and the unexcited medium. For these conditions, we have never succeeded to initiate or observe a solitary pulse.

For wave merging, solitary pulses exist but propagate at comparably small speeds as illustrated by the leading front in Fig. 1(b). The trailing waves are faster and vanish in close vicinity of the leading pulse. A similar difference in the velocities is found for stacking waves (Fig. 1(c)), however no pulse annihilation occurs. In this third case, trailing fronts decelerate as they approach a slow moving "frontier" pulse and adjust their velocity to the speed of their predecessor. This process creates dense wave packets that expand steadily as more and more pulses are incorporated. We note that an earlier study shows that the resulting shock line is well described by the Rankine–Hugoniot relation [18,19].

The formation of densely-stacked clusters can also occur in a more complex fashion. Fig. 2 shows a time–space plot of stacking waves for different experimental conditions. In this scenario, the waves stack via a cascade of bunching events. In Fig. 2, we initially observe the formation of several pulse doublets. Later these doublets appear to form larger pulse multiplets. This behavior has been observed also in numerical simulations by Rinzel et al. [5,20].

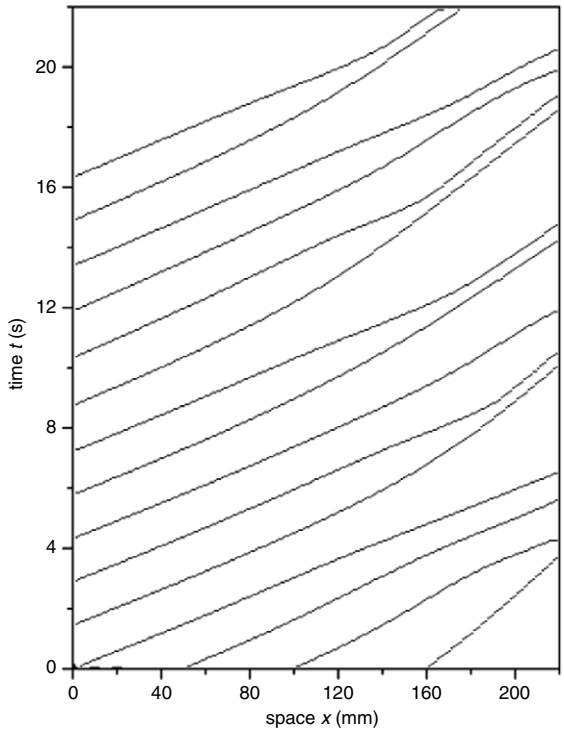

Fig. 2. Space–time trajectories of fronts in a system with bunching dynamics. Initial concentrations: $[H_2SO_4] = 2.0$ M, [CHD] = 0.15 M, $[NaBrO_3] = 0.14$ M, and [ferroin] = 0.50 mM.

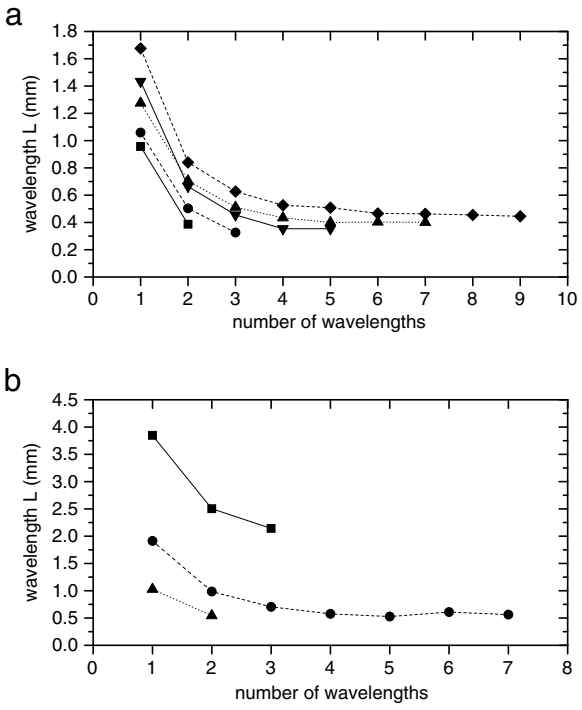

Fig. 3. Dependence of the stacking wavelength L on the number of the wavelength for various initial $NaBrO_3$ (a) and CHD-concentrations (b). Other initial concentrations are the same as in Fig. 1(a). $[NaBrO_3]$ in (a) are: ■ = 0.24 M, ● = 0.25 M, ▲ = 0.26 M, ▼ = 0.27 M, and ♦ = 0.28 M. In (b) the CHD-concentrations are ■ = 0.10 M, ● = 0.13 M, and ▲ = 0.15 M.

It can be interpreted as the creation of metastable pulse clusters that are mutually separated by increasingly large, and hence less unstable, distances.

A characteristic feature of wave stacking is the interpulse spacing within the stacked pulse multiplets. Qualitatively, this spacing can be interpreted as the wavelength L_0 for which the speed of a wave train equals the speed c_0 of a solitary pulse in a fully recovered medium. For large wavelengths L, the stability criterion is $\mathrm{d}c/\mathrm{d}L|_{L=L_0} > 0$ (see, for instance, [7]).

Closer inspection of our experimental data reveals small but systematic variations in L_0. For example, Fig. 1(c) clearly shows that the front spacing between the leading pulse $n = 1$ and its immediate successor $n = 2$ is larger than the distance between fronts 2 and 3. This phenomenon is quantified in Fig. 3 by plotting the time-independent spacing $L_n = x_{n+1}(t) - x_n(t)$ as a function of the pulse number n.

Fig. 3(a) shows L_n data for five different concentrations of the reactant $NaBrO_3$. For each concentration, L_n decreases with increasing values of n to level off at about 0.4 mm. Moreover, L_n increases systematically with increasing concentrations of $NaBrO_3$. A similar dependence is shown in Fig. 3(b) where three different concentrations of the organic substrate CHD are analyzed. Notice that L_n varies by a factor of nearly eight and that larger concentrations of CHD cause smaller stacking distances.

Overall, the data in Fig. 3 show that the pulse spacing in stacked wave clusters varies within its leading region. This variation decays rapidly with n and is pronounced only for the first three or four pulses. We emphasize that this dependence is *not* described by the simple kinematic criterion $c(L_0) = c_0$ and $\mathrm{d}c/\mathrm{d}L|_{L=L_0} > 0$.

4. Model and numerical integration results

4.1. Model

Earlier studies show that stacking, merging and tracking behavior can be found in a three-variable reaction–diffusion model [21,22]. In addition, it reproduces characteristic experimental observations such as firing sequences close to the stacking-merging transition and an obstacle-free nucleation mechanism of spiral waves in the merging regime. These findings suggest that the model captures the essential features of the wave dynamics in the CHD-BZ system. The model considers the spatio-temporal changes of one activator species u and two inhibitors referred to as v and w. In this Article, we consider a spatially one-dimensional version with one diffusive variable

$$\begin{aligned} u_t &= F(u, v, w) + u_{xx}, \\ v_t &= G(u, v, w), \\ w_t &= H(u, v, w). \end{aligned} \tag{1}$$

The rate laws are

$$\begin{aligned} F(u, v, w) &= \frac{1}{\epsilon} u(1-u)\left(u - \frac{v+w}{a}\right), \\ G(u, v, w) &= u - v, \\ H(u, v, w) &= \beta(\delta - w) - \gamma u w. \end{aligned} \tag{2}$$

The parameters ϵ, a, β, γ, and δ are dimensionless constants. For $\delta = 0$, Eqs. (1) and (2) are a specific case of the frequently studied Barkley model [23]. Moreover, Eqs. (1) and (2) are similar but not identical to the Krug model of the photosensitive BZ reaction [24], which itself is based on the classic Oregonator model [25]. These similarities suggest a possible interpretation of u, v and w as the concentrations of the chemical species $HBrO_2$, oxidized catalyst and Br^-, respectively.

Qualitatively, a typical unidirectional pulse in this model can be described as a propagating region of high u values in which the inhibitor w decreases while the inhibitor v increases. In its wake, these changes reverse and, thus, set up profiles that give rise to the aforementioned anomalies in the dispersion relation of wave trains. A convenient, and also intuitively approachable, bifurcation parameter is δ on which our analyses will concentrate. We note

that also negative values of δ are considered as they are relevant for understanding the origin of anomalous dispersion in this model. All other parameters are kept constant at

$$\epsilon = 1.0 \times 10^{-2}, \qquad a = 0.7, \qquad \beta = 0.3, \qquad \gamma = 5.0.$$

4.2. Numerical integration of full PDE

In this section, we present some results obtained by numerically integrating Eq. (1) using a forward Runge-Kutta time stepper of fourth order. The second derivative in space is approximated using a three-point stencil. No-flux (von Neumann) boundary conditions were imposed on both sides of the integration domain.

The phenomena of bunching, stacking, merging and tracking have been numerically reproduced with a high accuracy elsewhere (see, for instance, [21]). In Fig. 4(a) we revisit one of these findings for the example of four rightward traveling pulses which form a densely stacked wave packet. This stacking process is clearly due to the larger velocities of the three trailing pulses. Notice that the speed of the leading pulse is constant and identical to the velocity of the resulting, stable pulse quadruple. These dynamics can apparently be found for any number of pulses and in this respect the data in Fig. 4(a) are qualitatively similar to the experimental observations shown in Fig. 1(c). Note that the pulse quadruple is adsorbed by the no-flux boundary.

Now we focus on a new feature of bunching, namely on the local increase of the v inhibitor concentration prior to a bunching event. Fig. 4(b) shows space–time plots of Eq. (1) in one spatial dimension, which was periodically forced at one end by injecting new pulses into the medium. The example in Fig. 4(b) involves three distinctive bunching events in which pulses form pulse pairs (pay attention to the positions marked by arrows). One additional event causes pulse pairs to form a pulse quadruple. The latter case is marked by the letter Q in Fig. 4(b).

The interesting phenomenon resolved by this simulation is a local increase of v prior to the bunching event. Notice that this amplitude change occurs at all four bunching location in Fig. 4(b). Moreover, the value of the v variable remains larger than that of the leading (first) pulse in the pulse pair for all times after the bunching event. We suggest that the increase of the v variable during bunching events may be related to the nonequidistant wavelengths discussed in the context of the experimental Fig. 3.

Now we would like to compare our numerical finding to previously reported experimental results in which excitation pulses in a BZ system greatly increased their width while undergoing merging or tracking dynamics. In the corresponding time–space plots, such pulses create striking, trumpet-like traces (please compare Figs. 1 and 2 in [26]). This observation is another indication for changes in the v variable close to the location where two or more pulses begin to interact strongly and might hence be closely related to the amplitude shown in Fig. 4(b).

Although the phenomena of attractive pulse interaction can be easily verified in direct numerical simulations such as presented in Fig. 4, the underlying mechanism (and the question if there is any) of bunching and stacking in our model remains unresolved by the simulations. In the following section we are going to demonstrate that the attractive pulse interaction is indeed caused by a certain bifurcation, namely, by the orbit flip bifurcation of the homoclinic trajectory that describes the spatial profile of the solitary pulse. We will try to convince the reader that the orbit flip plays the role of an "organizing center" for the phenomena of attractive pulse interaction. Additionally, we will show that the phenomenon of tracking can also be traced down to a fold on the bifurcation line for the homoclinic orbit.

5. Traveling waves

The aim of this section is to provide an analysis, which is complementary to the previous experimental results and explicit time-stepping numerics by considering the so-called traveling waves, which propagate at a constant speed and with a constant profile. They can numerically be obtained as solutions of a certain ODE with a high degree of accuracy using a boundary-value problem solver.

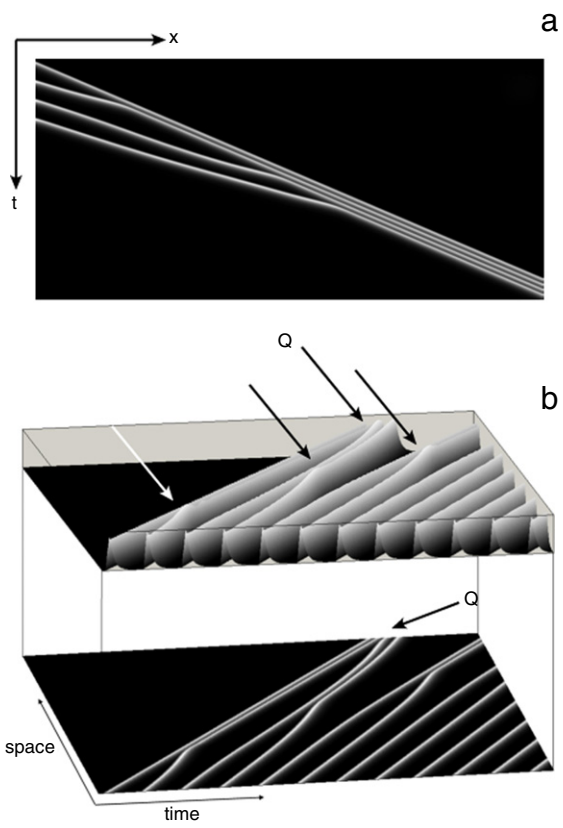

Fig. 4. (a) Time–space plot showing the stacking of four pulses to a stable wave packet obtained by numerical integration of Eqs. (1) and (2). The space and time axes span 800 and 500 units, respectively. The grey scale corresponds to the value of the v variable. The four pulses are initiated at the left system boundary with a time difference of 7.0 time units. With the exception of $\delta = 0.26$, all numerical and model parameters are given in the main text. (b) A more complicated stacking scenario involving additional pulses. The pulses are initiated at a period of 8.5 time units and $\delta = 0.265$. In the top portion, the spatio-temporal evolution of the variable v is also shown as surface heights revealing a local increase of v prior to the bunching events (marked by bold arrows). The two arrows labeled with letter Q mark the formation of a quadruple of pulses from two pulse pairs.

5.1. Traveling waves ODE

Introducing the co-moving coordinate system $x \to x - ct$ (c velocity of the frame), we obtain the existence equations for traveling waves

$$u_{xx} + cu_x + F(u, v, w) = 0,$$
$$cv_x + G(u, v, w) = 0,$$
$$cw_x + H(u, v, w) = 0,$$

which we cast as a system of four equations of the first order:

$$\begin{aligned} u_x &= U, \\ v_x &= -c^{-1}G(u, v, w), \\ w_x &= -c^{-1}H(u, v, w), \\ U_x &= -cU - F(u, v, w). \end{aligned} \tag{3}$$

A solitary pulse (periodic wave train of wavelength L) corresponds to a homoclinic trajectory (limit cycle of period L) in Eqs. (3). We search for those solutions in Eqs. (3) with the help of the continuation software AUTO 2000 [27]. Although a solitary pulse may have *several* high-amplitude peaks, we will refer to it as a

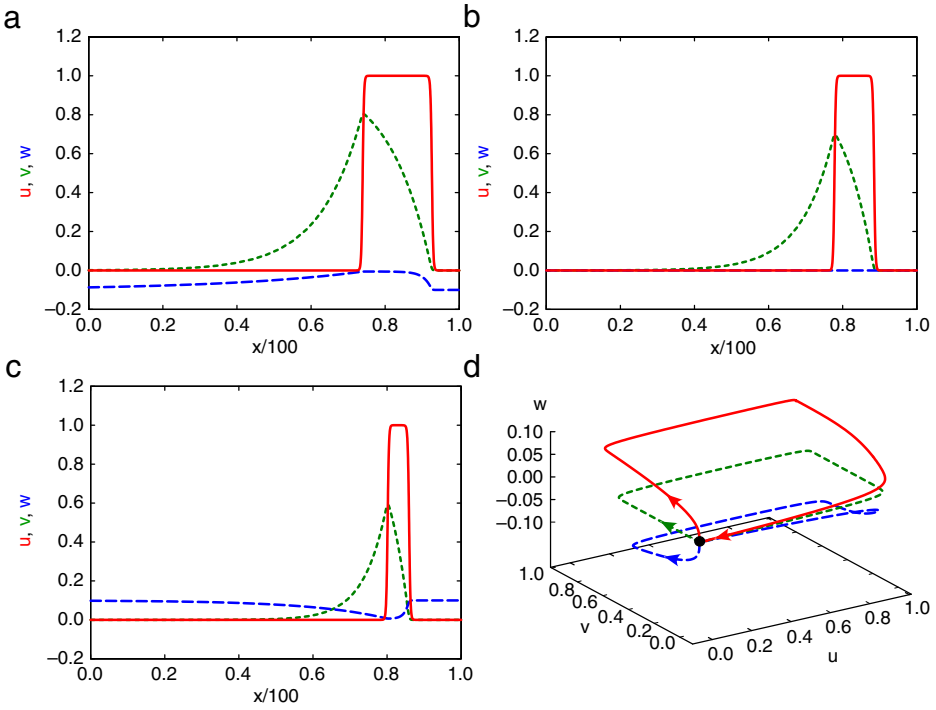

Fig. 5. Examples of pulse profile for $\delta = -0.1$ (a), $\delta = 0$ (b), and $\delta = 0.1$ (c). The red solid, green short-dashed, and blue long-dashed lines represent the variables u, v, and w, respectively. (d) Homoclinic connections for the above δ values in the three-dimensional (u, v, w) space. For clarity, the curves are shifted along the w axis placing their steady states at the origin. Here, the red solid, green short-dashed, and blue long-dashed curves correspond to $\delta = 0.1$, 0.0 and -0.1, respectively.

solitary one. This terminology stresses that the pulse is localized in space and does not occupy the entire 1D domain as in the case of spatially periodic wave trains. Notice that it differs slightly from the usage of the word in the earlier Sections. Furthermore, a solitary pulse has a unique propagation velocity c for every parameter set, whereas for periodic wave trains the propagation velocity c depends on the wavelength L. In the following, we continue to refer to the dependence $c = c(L)$ as the *dispersion* of the wave train.

Comparing the homoclinics in our model to others such as [5], let us emphasize here we are dealing with a homoclinic trajectory to a saddle equilibrium with purely real leading (the closest to the imaginary axis) eigenvalues. Thus, the wake of the pulse is monotonous and there are no small-amplitude oscillations behind it as in the case of homoclinics to a saddle-focus equilibrium.

5.2. Solitary pulses

Starting a continuation in parameter δ with a fixed point of Eqs. (3) $(u, v, w, U)^+ = (0, 0, \delta, 0)^+$ with the velocity $c = 3.0$ and $\delta = 1.0$, we detect several branches of equilibria and one of those undergoes a Hopf bifurcation at $\delta \approx -3.69 \times 10^{-3}$. From that point, we unfold a branch of limit cycles in Eqs. (3) performing continuation in the velocity c and the wavelength L. For large enough values of L, the periodic solution is used as a starting solution to compute a homoclinic solution, representing a solitary pulse in the reaction–diffusion system.

We find that depending on the sign of δ, solitary pulses have qualitatively different profiles. This result is illustrated in Fig. 5. The most important difference is the decay of the w variable behind the pulse. For negative δ, the w wake of the pulse approaches the asymptotic value $w = \delta$ from above (Fig. 5(a)) while for positive δ the w wake of the pulse approaches the asymptotic state $w = \delta$ from below (Fig. 5(c)). For the boundary value $\delta = 0$, the variable w does not show any dynamics at all but remains zero along the whole profile of the pulse (Fig. 5(b)). Also note the different widths of the u pulses in Fig. 5(a)–(c).

To obtain a better understanding of the δ-dependence of pulse dynamics, we plotted the homoclinics in a 3D phase space spanned by the three variables u, v and w (Fig. 5(d)). The graphs are generated for the same δ values explored in (a–c). For clarity, we shifted the homoclinic solutions in the w direction in such a way that the origin is always at $w = 0$. This is readily accomplished as the steady state is given by $u = v = 0$, $w = \delta$. Fig. 5 shows that for different values of δ, the homoclinics depart from the fixed point in either the positive or negative w direction. The return of the homoclinics, however, follows the same path for all δ.

From the viewpoint of dynamical systems, this change of the homoclinics configuration is known as *orbit flip* (see *e.g.*, Ref. [28]). An orbit flip is a codimension-two bifurcation, which means that it occurs for distinctive values of two parameters in Eqs. (3). In our case, these parameters are the propagation velocity of the pulse c and the model parameter δ which controls the behavior of w in the wake of the solitary pulse. Notice, however, that the parameter c is is not present in the original reaction diffusion Eqs. (1) but rather results from the traveling wave ansatz used to derive Eqs. (3). In experiments and numerical simulations of the full reaction–diffusion model, the pulse clearly selects its propagation velocity solely on the basis of the explicit model parameters. Hence, the orbit flip is controlled only by the parameter δ. Using the HOMCONT subroutines of AUTO [27], we find within the typical numerical accuracy the orbit flip at $\delta = 0$.

5.3. Periodic wave trains

Spatially periodic wave trains are parameterized by their wavelength, or equivalently spatial period, L. The propagation velocity of a wave train depends on L, thus, resulting in a dispersion $c = c(L)$, which can also be multi-valued. As a rule, there is a well-defined limit for $L \to \infty$, namely the propagation velocity of the solitary pulse. For large wavelengths, the slope of dispersion determines how pulses interact inside a wave train: a positive slope reflects the repulsive interaction of pulses and, thus, stability

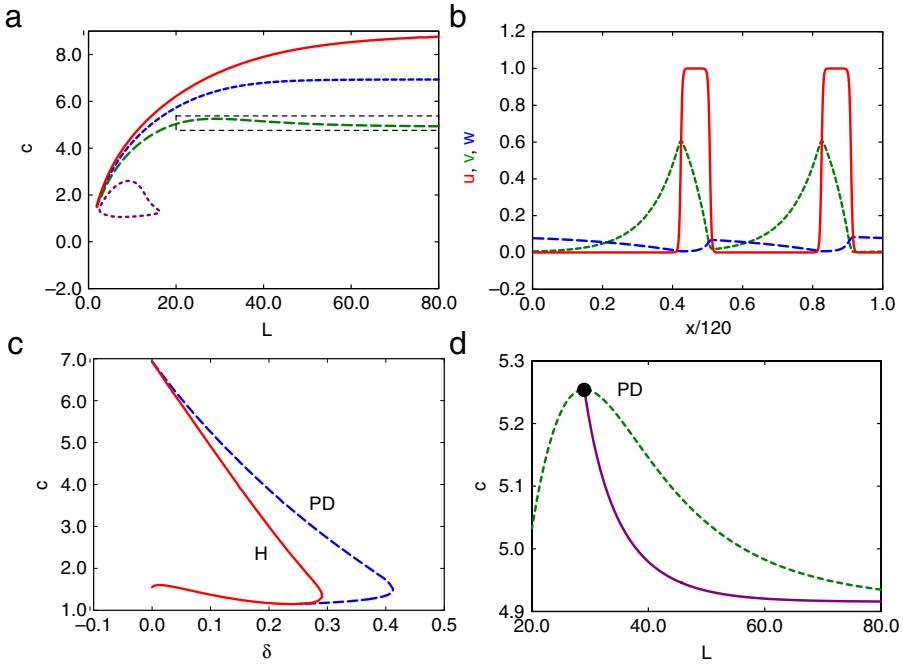

Fig. 6. (a) Dispersion curves for $\delta = -0.1$ (solid red line), $\delta = 0.0$ (short-dashed blue line), $\delta = 0.1$ (long-dashed green line), and $\delta = 0.3$ (closed dashed line). (b) Profile of a period-2 wave train for $\delta = 0.1$ with a wavelength of $L = 120$. The red solid, green short-dashed, and blue long-dashed lines correspond to the variables u, v, and w, respectively. (c) Velocity of solitary pulses (continuous red line) and period-doubled wave trains (blue dashed) as a function of the parameter δ. (d) Magnification of dashed box in (a) showing the overshooting, primary dispersion curve for $\delta = 0.1$ (long-dashed green line) and the dispersion curve of period-doubled wave trains (continuous purple line).

of the whole wave train whereas a negative slope in the dispersion means attractive interaction of pulses and instability of the wave train (see [29,30] and references therein).

For $\delta < 0$, the dispersion curve of wave trains in Eqs. (1) has positive slopes. A representative example is shown as the red curve in Fig. 6(a). However, the orbit flip bifurcation for the solitary pulses at $\delta = 0$ has a profound impact on the dispersion of spatially periodic wave trains. For $\delta > 0$, there is an overshoot in the dispersion curve. This case is exemplified by the green line in Fig. 6(a) and further illustrated in Fig. 6(d). A part of the dispersion with large L has a negative slope. Moreover, there is a period-doubling bifurcation close to the apex of the dispersion curve for $\delta > 0$. This point is labeled 'PD' in Fig. 6(d). At that point, a new branch of spatially periodic wave trains bifurcates. In these wave trains, every spatial period contains two high-amplitude maxima. A typical example is shown in Fig. 6(b). Note that here we cannot see a difference in the maximal values of the v variable in the first and second pulse in the pulse pair contrary to Fig. 4. Both branches of the bifurcated dispersion curve have negative slope. For large wavelengths, the branch of doubled wave trains asymptotically approaches the curve describing solitary pulse pairs.

For a monotonic dispersion relation, such as the red curve in Fig. 6(a), the fastest wave train is of infinite wavelength. This case is identical to the solitary pulse solution. However, if there is an overshoot in the dispersion, the wavelength of the fastest wave train is finite. The existence domain of periodic wave trains with finite wavelength and that of solitary pulses differ. To illustrate this important finding, we plot in Fig. 6(c) the δ-dependence of the velocity of solitary pulses (red line) and period-doubling wave trains (blue dashed line). Note that both red and blue curves are double-valued, i.e. there are two velocity values for certain δ. One usually expects the slower one to be unstable. This topic has been discussed rigorously by others for similar models such as the FitzHugh–Nagumo equations [31]. Whereas the slow unstable pulse and pulse trains cannot be observed experimentally, their existence is quite important: The point in the parameter space where the fast and the slow pulses meet is a fold point and no pulses exist beyond it. Thus, the point of transition between the fast stable and the slow unstable pulses defines the extinction threshold for one-dimensional pulse propagation.

The most interesting feature of the results in Fig. 6(c) is that the turning points of the blue ($\delta = 0.42$) and the red curve ($\delta = 0.29$) do not occur at the same δ value. Accordingly there is a range of values $0.29 < \delta < 0.42$ for which certain wave trains with finite wavelengths but no solitary pulses exist. This finding is very closely related to the fact that the purple dispersion curve in Fig. 6(a) ($\delta = 0.3$) occupies a finite band of wavelengths and does not extend to $L = \infty$. Propagation of periodic wave trains of finite wavelengths combined with the lack of solitary pulses is clearly identical to the *pulse tracking* behavior shown in Fig. 1(a).

The negative slope of the primary dispersion curve and the emergence of period-doubled wave trains are intrinsically related. Indeed, for dispersions with negative slope, an equally spaced wave train is unstable to spatial shifts of individual pulses. For example, pushing a pulse in the forward direction increases its speed, since the interpulse distance to the preceding pulse has decreased. Consequently, the wave train breaks into pulse pairs. Also the negative slope of the doubled dispersion suggests that interaction between pulse pairs is attractive. This attractive interaction between individual pulses and/or pulse pairs in a wave train also leads to the formation of pulse triples, quadruples, etc. These phenomena match our experimental observations of *pulse stacking* and *pulse bunching*, which are shown in Figs. 1(c), 2, and 4.

In conclusion, we have shown that an orbit flip bifurcation for solitary pulses in Eqs. (1) at $\delta = 0$ causes the overshoot in the dispersion curve of spatially periodic wave trains and the emergence of period-doubled wave trains and pulse pairs. This bifurcation of solitary pulses explains the *stacking* and *tracking* dynamics discussed in Section 3 and earlier publications [21]. However, the explanation of the third experimentally observed phenomenon, *pulse merging*, requires additional results that will be described in the following.

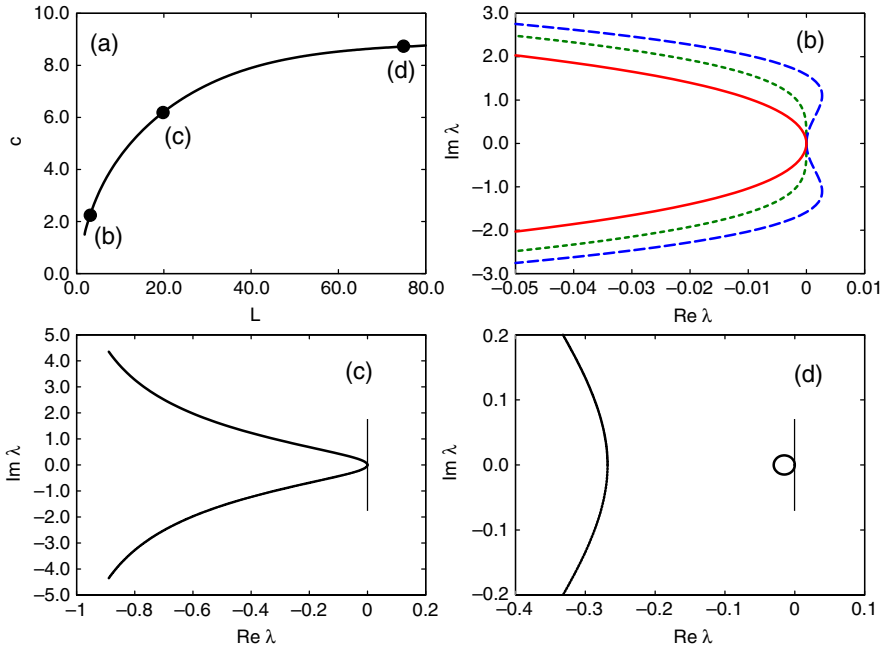

Fig. 7. (a) Dispersion curves for $\delta = -0.1$. Locations (b)–(d) denotes the points on the dispersion, for which spectra are shown in (b)–(d). (b) Three spectra close to mark (b) in frame (a) revealing a long-wavelength instability at wavelength $L = 3.06$. The solid red line shows the spectrum for L slightly larger than the critical one. The short-dashed green line shows the spectrum in the critical point with zero tangency at the origin, The long-dashed blue line shows the spectrum for L slightly smaller than $L = 3.06$. (c) Spectrum for mark (c) in (a). (d) Spectrum for mark (d) in (a). Notice the location of the circle which indicates stability the of wave trains. In (c) and (d), the vertical dash denotes the boundary $\mathrm{Re}\,\lambda = 0$.

6. Stability results

6.1. Formulation of eigenvalue problem

Suppose we have an L-periodic wave train $(u, v, w)(x) = (u, v, w)(x + L)$. In order to compute its spectrum, we formulate the following eigenvalue problem

$$\begin{aligned} &\bar{u}_{xx} + c\bar{u} + F_u\bar{u} + F_v\bar{v} + F_w\bar{w} = \lambda\bar{u},\\ &c\bar{v} + G_u\bar{u} + G_v\bar{v} + G_w\bar{w} = \lambda\bar{v},\\ &c\bar{w} + H_u\bar{u} + H_v\bar{v} + H_w\bar{w} = \lambda\bar{w} \end{aligned} \tag{4}$$

for the unknown complex-valued eigenfunction $(\bar{u}, \bar{v}, \bar{w})$ and the eigenvalue λ. This set of equations is the linearization of Eqs. (1) in the moving coordinate system and capitals with a subscript denote the linearization of the nonlinear kinetics of Eqs. (1), evaluated along the profile of the wave train $(u, v, w)(x)$. If we consider Eq. (4) for the boundary conditions

$$(\bar{u}, \bar{v}, \bar{w})(L) = \mathrm{e}^{\mathrm{i}2\pi\gamma}(\bar{u}, \bar{v}, \bar{w})(0), \tag{5}$$

then λ is in the spectrum of wave train if Eqs. (4) and (5) have a solution for a real γ [32]. The spectrum λ comes in curves, parameterized by the wavenumber γ. Thus it is possible to compute it numerically by performing continuation in γ, starting from a known solution, for instance, from the Goldstone mode, which is given by the derivative of the wave train itself and $\lambda = \gamma = 0$.

The wave train is stable, if all eigenvalues λ are contained in the left complex half-plane with the exception of the Goldstone eigenvalue at the origin. However, if some of the eigenvalues are in the right half-plane, the wave train is unstable. The stability of wave trains depends on the choice of domain and the boundary conditions [33].

The spectrum of solitary pulses with isolated point eigenvalues can be approximated by the spectrum of wave trains with large spatial period [29]. Every point eigenvalue of the solitary pulse is approximated by a small piece (usually a circle) of the continuous spectrum of the wave train. In particular, we are interested in the so-called *circle of critical eigenvalues*, which is attached to the origin of the complex plane being the blow-up of the Goldstone eigenvalue of the solitary pulse. This circle reflects the stability of the wave train with respect to shifts of individual pulses that constitute the wave train.

For large wavelengths, the location of the circle is related to the slope of the dispersion: for a positive slope the circle opens in the left half-plane, showing the stability of the wave train and for a negative slope, the circle opens in the right-half plane reflecting instability.

Notice that the circle depends on the stability of wave trains in an infinitely large, unbounded domain. Truncating the domain by imposing periodic boundary conditions causes the curves to break up into point eigenvalues. The spectrum of N pulses, which are equidistantly placed on a ring with periodic boundary conditions will show exactly N eigenvalues located on the continuous spectrum (*i.e.*, the aforementioned circle) of the unbounded problem. In other words, setting γ to $\frac{n}{N}$, $n = 1, 2, \ldots, N-1$ results in eigenfunctions with periods being multiples of the period of the wave train.

6.2. Wave train stability for $\delta < 0$

For negative values of δ, the dispersion of wave trains displays a positive slope. It is interesting that there is no slower unstable pulse for negative δ and the dispersion does not contain a slower branch, in contrast to the usual situation with two branches of dispersion for every value of the control parameter.

The only instability of wave trains occurs at a small wavelength $L \approx 3.06$ (see Fig. 7(a) and (b)). In the critical point, the leading part of the spectrum has zero curvature at the origin and for $L < 3.06$ it crosses into the right complex half-plane, reflecting the instability of the wave trains. Notice that the eigenvalues closest to zero cross first. These eigenvalues have small γ and, hence, the unstable modes have large wavelengths.

For larger wavelengths, all wave trains are stable, as illustrated by the spectra in Fig. 7(c) and (d). The spectrum in Fig. 7(c) is a

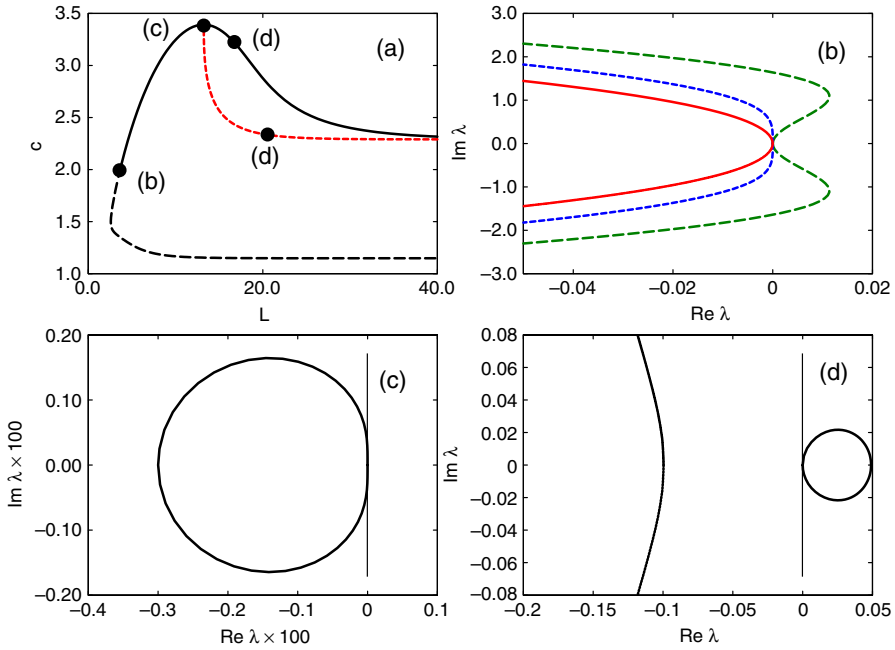

Fig. 8. (a) Dispersion curves for $\delta = 0.24$. Locations (b)–(d) denote the points for which spectra are plotted in (b)–(d). The short-dashed red line shows the dispersion curve of period-doubled wave trains. The long-dashed part of the black curve is the unstable segment of the primary dispersion. (b) Three spectra close to mark (b) in frame (a) showing a long-wavelength instability at wavelength $L \approx 3.8$. The solid red line shows the spectrum for L slightly larger than the critical one, while the short-dashed blue line shows the spectrum in the critical point with a zero tangency at the origin. The long-dashed green line is a spectrum for L slightly smaller than $L = 3.8$. (c) Spectrum for mark (c) close to the period-doubling bifurcation in (a). Note the zero tangency at the origin. (d) Spectrum for mark (d) on the black branch in (a). The spectrum for mark (d) on the red dashed branch in (a) is qualitatively the same and the circle is also found in the positive half-plane. In (c) and (d) the vertical dash denotes the boundary $\mathrm{Re}\,\lambda = 0$.

typical curve attached to the origin, whereas in (d) a part of the spectrum detaches from the rest and forms the aforementioned circle of critical eigenvalues. The circle is attached to the origin, as implied by the translational symmetry of the problem, and opens into the left half-plane, showing the stability of wave trains. Upon further increase of wavelength L that circle shrinks to the point eigenvalue at zero at an exponential rate in L, as rigorously proven in [29].

In summary, for negative values of δ the majority of wavelengths shows stability of wave trains. This case turns out to be the simplest one.

6.3. Stability in the stacking regime

Increasing δ beyond zero causes a qualitative change in the dispersion curve as shown in Fig. 8(a). The curve has a pronounced overshoot and negative slopes for large wavelengths. Accordingly, the asymptotic velocity of the solitary pulse is approached from above.

Close to the overshoot, the leading (right-most) part of the spectrum is nearly a circle. In point (c) in Fig. 8(a), the wave train loses stability similarly to the short-wavelength instability observed above. The tangency of the spectrum at the origin becomes zero (see Fig. 8(c)) and a part of the circle crosses into the right-half plane. Close to that point, a branch of period-doubled wave trains bifurcates from the primary dispersion (red dashed line in Fig. 8(a)).

Beyond the overshoot, the circle of critical eigenvalues is located in the right complex half-plane. This situation is illustrated in Fig. 8(d). Again, upon increasing L the circle shrinks to a point eigenvalue at the origin. Another part of the spectrum, however, remains in the left half-plane.

Usually, the spectrum of the bifurcating period-doubled wave trains resembles that of the primary wave train in the sense that it also contains a circle of critical eigenvalues in the right half-plane. Qualitatively, the spectrum is similar to that shown in Fig. 8(d). The instability of the period-doubled wave trains is again due to attractive interaction between pairs – at least, for large wavelength L this can be read off from the negative slope of the period-doubled wave train dispersion $c = c(L)$ – and all considerations on the relation between the slope of the dispersion and the stability apply also for period-doubled waves. Analogously to the formation of pulse pairs, the attraction between pairs is likely to induce the formation of pulse quadruples.

The case of $\delta > 0$ differs from the behavior for $\delta < 0$ also with regard to the slower branch of the dispersion curve. As shown in Fig. 8(a), this branch also asymptotically approaches a solitary pulse, which is, however, unstable. The loss in stability along the dispersion at smaller wavelengths occurs in a similar manner as for $\delta < 0$ through a zero-tangency situation at the origin (see Fig. 8(b)).

The distinguishing stability feature in the stacking regime is that for wavelengths beyond the apex of the overshoot, the circle of critical eigenvalues is located in the right half-plane. This instability is caused by the attractive interaction between (at least) two pulses and, thus, does not occur for a single pulse on a ring. The most unstable mode belonging to the right-most point of the circle is found for $\gamma = 0.5$, which implies that the corresponding eigenfunction has twice the wavelength of the wave train.

Also note that the velocity of the short-wavelength instability (b) in Fig. 8(a) is below the velocity of the solitary pulse. Hence, solitary pulses *can coexist* with periodic wave trains of the equal velocity. This is not the case in the *merging* regime, as described in the following subsection.

6.4. Stability in the merging regime

The merging regime, analyzed here for $\delta = 0.28$, is characterized by the fact that periodic wave trains and solitary pulses cannot coexist and co-propagate at the same velocity as in the stacking regime. Indeed, the stability onset in the short-wavelength region is above the velocity of solitary pulses (see Fig. 9). The only stable wave trains have velocities that are larger than the velocity of the solitary pulse and, hence, they approach

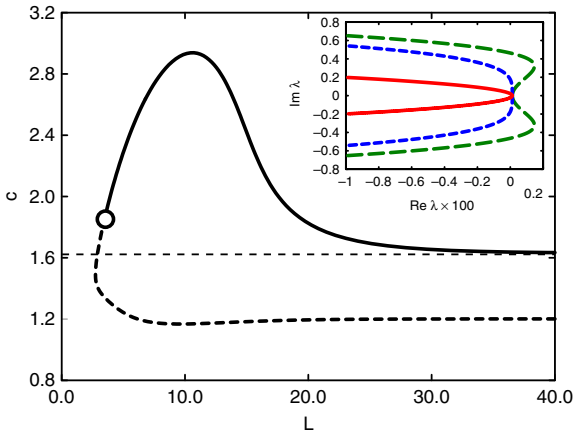

Fig. 9. Main frame: dispersion of wave trains for $\delta = 0.28$. Open dot denotes the instability point. Horizontal straight line shows the velocity of solitary pulse. Dashed line denotes the unstable segment of dispersion. Inset: spectra at the location of open dot in the main frame. Solid red line denotes stable spectra, blue short-dashed line denotes spectrum at the onset of instability and long-dashed green line denotes spectrum of unstable wave train.

the solitary pulse and cause front-to-back collisions. However, as they approach the slower solitary pulse, they effectively acquire a smaller wavelength, enter the unstable region in the dispersion in Fig. 9, and eventually break up due to the instability.

Considering the stability of wave trains close to the apex of the dispersion and the emergence of double-spaced wave trains, we find qualitatively the same results as reported for $\delta = 0.24$.

7. Conclusions

Solitary excitation pulses and wave trains exist in a great variety of experimental systems and often show remarkable universalities and surprising complexity. While these phenomena are most striking in spatially two- and three-dimensional media, complex dynamics and interesting instabilities can also be found in the simpler one-dimensional case. Here, we presented observations obtained from experiments with the CHD-BZ reaction that show at least three qualitatively different types of wave dynamics, that we refer to as stacking, merging and tracking. Moreover, systematic surveys of this reaction system show that these dynamics are encountered for all, or at least an extremely wide range, of initial concentrations. Earlier studies have linked these features to anomalous (*i.e.*, non-monotonic) dispersion and reproduced qualitatively many of the experimental observations in a three-variable reaction–diffusion model. However, numerical integrations of the model equations (Eqs. (1) and (2)) are not capable of revealing the underlying bifurcations and instabilities.

This shortfall has been addressed by our study providing deeper insights into the aforementioned model, which most likely also apply to the CHD-BZ system. These findings can be summarized as follows:

- *Normal dispersion* of periodic wave trains is observed in Eqs. (1) and (2) for $\delta < 0$. Pulse trains are stable and their interaction is repulsive. No stationary multipulse configurations are possible. Solitary pulses are the fastest waves.
- *Pulse stacking* is caused by the overshoot in the dispersion relation and the existence of the negative slope domain in it. As a result, pulses in a wave train interact attractively and form pulse pairs and multiplets. There exist wave trains with finite wavelength that propagate faster than the solitary pulse. Those periodic wave trains are located close to the overshoot in the dispersion. Necessary for pulse stacking is the existence of *stable* periodic wave trains traveling at the same velocity as the solitary pulse.
- *Pulse merging* can be understood by looking at the stability onset of periodic wave trains in the region of small wavelengths. Wave trains with the same velocity as solitary pulses are now *unstable* and, thus, break up once the interpulse distance is in the unstable region.
- *Pulse tracking* is characterized by the non-existence of solitary pulses. However, periodic wave trains with finite wavelengths do exist and their dispersion relation forms a closed curve.

Furthermore, we showed that the transition from normal dispersion for $\delta < 0$ to the dispersion with an overshoot for $\delta > 0$ is due to an orbit flip bifurcation of the homoclinic orbit describing the solitary pulse. This change in the dispersion slope followed by the change in the wave train stability is a generic phenomenon near flips of homoclinics and has been reviewed in [30]. For the CHD-BZ reaction, it is not fully clear whether normal dispersion can actually be observed, as stacking behavior with an overshoot at very large wavelength is extremely difficult to distinguish from true normal dispersion. However, an earlier study reported good evidence for normal dispersion under reaction conditions involving low bromate and high CHD concentrations [12].

We also re-emphasize that both *stacking* and *tracking* can be explained with the help of Eq. (3). In contrast, to understand *merging* it is important to have the stability information about the wave train in the short-wavelength region. Nevertheless, the dynamics resulting from the earlier two wave regimes are equally interesting from the viewpoint of wave stability. Lastly, there are additional features of the experimental systems, such as the non-uniformly spaced wave trains described in Fig. 3 that require further investigation.

Considering the experimental significance of the presented results, we would like to refer to [34], where phenomena similar to stacking and merging were reported for a chemical setup different from that of Manz et al. [21], thus suggesting a generic nature of the effects reported in this paper.

Acknowledgements

This work has been supported by the National Science Foundation under Grant No. 0513912 and the Deutsche Forschungsgemeinschaft through Sfb 555.

References

[1] R. Kapral, K. Showalter (Eds.), Chemical Waves and Patterns, Kluwer, Dordrecht, Netherlands, 1995;
M.C. Cross, P.C. Hohenberg, Rev. Modern Phys. 65 (1993) 851.
[2] M. Kim, et al., Science 292 (2001) 1357;
A.N. Zaikin, A.M. Zhabotinsky, Nature 225 (1970) 535;
K. Agladze, O. Steinbock, J. Phys. Chem. A104 (2000) 9816;
S.C. Müller, T. Mair, O. Steinbock, Biophys. Chem. 72 (1998) 37;
A.M. Pertsov, J.M. Davidenko, R. Salomonsz, W.T. Baxter, J. Jalife, Circ. Res. 72 (1993) 631;
N. Suzuki, M. Hirata, S. Kondo, Proc. Natl. Acad. Sci. USA 100 (2003) 9680.
[3] J.D. Dockery, J.P. Keener, J.J. Tyson, Physica D30 (1988) 177;
O. Steinbock, S.C. Müller, Physica A188 (1992) 61.
[4] J.-M. Flesselles, A. Belmonte, V. Gáspár, J. Chem. Soc. Faraday Trans. 94 (1998) 851.
[5] C. Elphick, E. Meron, E.A. Spiegel, Phys. Rev. Lett. 61 (1988) 496;
C. Elphick, E. Meron, J. Rinzel, E.A. Spiegel, J. Theoret. Biol. 146 (1990) 249.
[6] M. Or-Guil, J. Krishnan, I.G. Kevrekidis, M. Bär, Phys. Rev. E 64 (2001) 046212.
[7] M. Or-Guil, I.G. Kevrekidis, M. Bär, Physica D 135 (2000) 154.
[8] A.T. Winfree, Physica D49 (1991) 125.
[9] M. Falcke, M. Or-Guil, M. Bär, Phys. Rev. Lett. 84 (2000) 4753;
G. Bordiougov, H. Engel, Phys. Rev. Lett. 90 (2003) 148302;
G. Roder, G. Bordyugov, H. Engel, M. Falcke, Phys. Rev. E75 (2007) 036202.
[10] S. Jakubith, et al., Phys. Rev. Lett. 65 (1990) 3013;
J. Christoph, et al., Phys. Rev. Lett. 82 (1999) 1586.
[11] N. Manz, S.C. Müller, O. Steinbock, J. Phys. Chem. A104 (2000) 5895.
[12] C.T. Hamik, N. Manz, O. Steinbock, J. Phys. Chem. A105 (2001) 6144.
[13] F. Siegert, C. Weijer, J. Cell. Sci. 93 (1989) 325.
[14] A. Yochelis, E. Knobloch, Y. Xie, Z. Qu, A. Garfinkel, EPL 83 (2008) 64005.
[15] M. Stich, A.S. Mikhailov, Y. Kuramoto, Phys. Rev. E 79 (2009) 026110.

[16] K. Kurin-Csörgei, A.M. Zhabotinsky, M. Orbán, I.R. Epstein, J. Phys. Chem. 100 (1996) 5393;
K. Kurin-Csörgei, A.M. Zhabotinsky, M. Orbán, I.R. Epstein, J. Phys. Chem. A101 (1997) 6827.
[17] T. Yamaguchi, L. Kuhnert, Z. Nagy-Ungvarai, S.C. Müller, B. Hess, J. Phys. Chem. 95 (1991) 5831;
B.T. Ginn, B. Steinbock, M. Kahveci, O. Steinbock, J. Phys. Chem. A108 (2004) 1325.
[18] C.T. Hamik, O. Steinbock, Phys. Rev. E65 (2002) 046224;
N. Manz, O. Steinbock, Phys. Rev. E70 (2004) 066213.
[19] B. Sandstede, A. Scheel, SIAM J. Appl. Dyn. Syst. 3 (2004) 1.
[20] J. Rinzel, K. Maginu, in: C. Vidal, A. Pacault (Eds.), Nonequilibrium Dynamics in Chemical Systems, Springer, Berlin, 1984, pp. 107–113.
[21] N. Manz, C.T. Hamik, O. Steinbock, Phys. Rev. Lett. 92 (2004) 248301.
[22] N. Manz, B.T. Ginn, O. Steinbock, Phys. Rev. E73 (2006) 066218.
[23] D. Barkley, Physica (Amsterdam) 49D (1991) 61.
[24] H.J. Krug, L. Pohlmann, L. Kuhnert, J. Phys. Chem. 94 (1990) 4862.
[25] R.J. Field, R.M. Noyes, J. Chem. Phys. 60 (1974) 1877.
[26] N. Manz, O. Steinbock, Chaos 16 (2006) 037112.
[27] E. Doedel, R.C. Paffenroth, A.R. Champneys, T.F. Fairgrieve, Yu.A. Kuznetsov, B.E. Oldemann, B. Sandstede, X. Wang, AUTO2000: Continuation and bifurcation software for ordinary differential equations (with HOMCONT), Concordia University, Montreal (2002).
[28] Yu.A. Kuznetsov, Elements of Applied Bifurcation Theory, Springer, Berlin, 1995.
[29] B. Sandstede, A. Scheel, J. Differential Equations 172 (2001) 134.
[30] B. Sandstede, Stability of travelling waves, in: B. Fiedler (Ed.), Handbook of Dynamical Systems, Vol. 2, North-Holland, 2002.
[31] M. Krupa, B. Sandstede, P. Szmolyan, J. Differential Equations 133 (1997) 49.
[32] J.D.M. Rademacher, B. Sandstede, A. Scheel, Physica D 229 (2007) 166.
[33] B. Sandstede, A. Scheel, Physica D 145 (2000) 233.
[34] M. Harati, J. Wang, Chaos 19 (2009) 023116.